ACS APPLIED MATERIALS & INTERFACES

Research Article

www.acsami.org

Electrophoretic Deposition of Dexamethasone-Loaded Mesoporous Silica Nanoparticles onto Poly(L-Lactic Acid)/Poly(ε-Caprolactone) Composite Scaffold for Bone Tissue Engineering

Kexin Qiu,[†,‡] Bo Chen,[§] Wei Nie,[†] Xiaojun Zhou,[†,‡] Wei Feng,[†] Weizhong Wang,[†] Liang Chen,[†] Xiumei Mo,[†,‡] Youzhen Wei,[∥] and Chuanglong He*[,†,‡]

[†]College of Chemistry, Chemical Engineering and Biotechnology; State Key Laboratory for Modification of Chemical Fibers and Polymer Materials, Donghua University, 2999 North Renmin Road, Shanghai 201620, China

[‡]College of Materials Science and Engineering, Donghua University, Shanghai 201620, China

[§]Department of Radiology, Shanghai East Hospital, Tongji University School of Medicine, Shanghai 200120, China

[∥]Reserch Center for Translational Medicine, Shanghai East Hospital, Tongji University, Shanghai 200120, China

Supporting Information

ABSTRACT: The incorporation of microcarriers as drug delivery vehicles into polymeric scaffold for bone regeneration has aroused increasing interest. In this study, the aminated mesoporous silica nanoparticles (MSNs-NH_2) were prepared and used as microcarriers for dexamethasone (DEX) loading. Poly(L-lactic acid)/poly(ε-caprolactone) (PLLA/PCL) nanofibrous scaffold was fabricated via thermally induced phase separation (TIPS) and served as template, onto which the drug-loaded MSNs-NH_2 nanoparticles were deposited by electrophoretic deposition (EPD). The physicochemical and release properties of the prepared scaffolds (DEX@MSNs-NH_2/PLLA/PCL) were examined, and their osteogenic activities were also evaluated through in vitro and in vivo studies. The release of DEX from the scaffolds revealed an initial rapid release followed by a slower and sustained one. The in vitro results indicated that the DEX@MSNs-NH_2/PLLA/PCL scaffold exhibited good biocompatibility to rat bone marrow-derived mesenchymal stem cells (BMSCs). Also, BMSCs cultured on the DEX@MSNs-NH_2/PLLA/PCL scaffold exhibited a higher degree of osteogenic differentiation than those cultured on PLLA/PCL and MSNs-NH_2/PLLA/PCL scaffolds, in terms of alkaline phosphatase (ALP) activity, mineralized matrix formation, and osteocalcin (OCN) expression. Furthermore, the in vivo results in a calvarial defect model of Sprague−Dawley (SD) rats demonstrated that the DEX@MSNs-NH_2/PLLA/PCL scaffold could significantly promote calvarial defect healing compared with the PLLA/PCL scaffold. Thus, the EPD technique provides a convenient way to incorporate osteogenic agents-containing microcarriers to polymer scaffold, and thus, prepared composite scaffold could be a potential candidate for bone tissue engineering application due to its capacity for delivery of osteogenic agents.

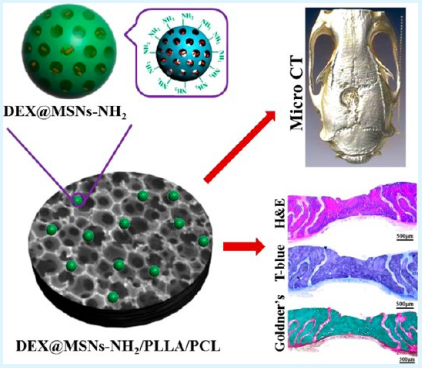

KEYWORDS: *electrophoretic deposition, mesoporous silica nanoparticles (MSNs), dexamethasone, poly(L-lactic acid)/poly(ε−caprolactone) scaffold, bone tissue engineering*

1. INTRODUCTION

Treatment of bone defects is still a significant clinical challenge since autografts and allografts are limited due to their decreased use and some associated donor site morbidity.[1,2] Bone tissue engineering, which combines osteogenic cells, osteoconductive scaffolds, and osteogenic agents together in an orchestrated way, has emerged as a promising approach to constructing the bone alternatives for bone regeneration.[3] Ideally, bone scaffold should not only provide structural support for embedded cells but also deliver osteogenic agents to regulate cellular responses and trigger tissue repair.[4−8] To this end, it is desirable to create scaffolds with the capability of controllably releasing osteogenic agents. However, direct incorporation of osteogenic agents into the polymeric scaffold might potentially result in undesired burst release and denaturation of these osteogenic agents due to exposure to harsh preparation conditions. The limitation of conventional monolithic scaffold can be overcome by introducing microcarriers (microspheres or nanospheres) as drug delivery vehicles into the bulk scaffold, which not only provides protection for the encapsulated bioactive molecules during scaffold fabrication but also allows the scaffold to provide both structural support and controlled release properties.[9]

Received: December 6, 2015
Accepted: January 6, 2016
Published: January 6, 2016

DOI: 10.1021/acsami.5b11879
ACS Appl. Mater. Interfaces 2016, 8, 4137−4148

Biomimetic nanofibers have been developed as promising tools for constructing biomimetic scaffolds to promote tissue regeneration due to their ability to mimic the nanoscale structure of native extracellular matrix (ECM).[10,11] Among different nanofiber fabrication techniques, thermally induced phase separation (TIPS) is a well-known method to fabricate porous nanofibrous scaffolds that are most suitable for bone tissue engineering applications.[12,13] However, the harsh conditions for phase separation may cause additional difficulties in introducing drug delivery systems into a porous scaffold during the fabrication process due to the risk of destroying the bioactive agents. Alternatively, the incorporation of bioactive agents-containing microcarriers into the nanofibrous scaffold has been proven to be an effective way of endowing scaffold with the capability of controlling the release of bioactive agents.[14]

Mesoporous silica nanoparticles (MSNs) are a highly promising drug carrier due to their high specific surface areas, large pore volumes, high loading capacity, and favorable biocompatibility.[15−18] Moreover, their silanol-containing surface can be functionalized with suitable organic molecules, allowing a better control over the release of bioactive agents which can be incorporated into both the mesoporous channels of MSNs and organic coating. In this sense, MSNs can be developed to be very promising microcarriers for delivery of osteogenic agents for bone regeneration.

The microcarrier-based drug delivery system can be directly incorporated into the interior of the scaffold during fabrication or immobilized on the surface of the scaffold after fabrication. In contrast, the immobilization of microcarriers onto the surface of the scaffold can provide a scaffold with a controlled drug-release profile without compromising the properties of the bulk scaffold. While incorporation of polymeric microcarriers onto the surface of the scaffold can be achieved by covalently linking microcarriers with bulk scaffold, the incorporation of inorganic microcarriers onto the scaffold still possesses difficulties mainly due to the lack of organic functional groups on the surface of inorganic microcarriers. Electrophoretic deposition (EPD) is an effective approach to generate coating on the surface of metallic or polymeric substrates.[19−22] Commonly, EPD was adopted to deposit minerals or particles on the metallic substrates (e.g., stainless steel, titanium, and magnesium alloys).[19,23−25] Our previous studies have demonstrated the feasibility of applying the electrodeposition technique to form a calcium phosphate coating on the surface of the polymeric scaffold.[26−28] Therefore, we hypothesized that bioactive molecules-containing microcarriers could be deposited onto the polymer scaffold by the EPD technique, thus creating a bioactive composite scaffold for bone regeneration.

Herein, we utilize the well-established EPD technique to incorporate the MSNs-based carrier system to the polymeric scaffold. Poly(L-lactic acid)/poly(ε-caprolactone) (PLLA/PCL) nanofibrous scaffolds were fabricated by means of TIPS technique. Specially, the PLLA/PCL scaffold with controllable size and improved strength could be fabricated with appropriate molds, which is more suitable for human use. Dexamethasone (DEX), which could promote the osteoblast differentiation and enhance the alkaline phosphatase (ALP) activity and bone mineralization,[29−31] was chosen as the osteogenic molecule and loaded into aminated MSNs (MSNs-NH_2). The obtained DEX@MSNs-NH_2 microcarriers were subsequently deposited to the PLLA/PCL scaffold by EPD. The physicochemical and drug release properties of the composite scaffold were investigated, and their osteogenic activities were also evaluated through in vitro and in vivo studies.

2. EXPERIMENTAL SECTION

2.1. Fabrication of DEX@MSNs-NH_2. MSNs were synthesized as in a previously described method.[32] Briefly, 1.0 g of cetyltrimethylammonium bromide (CTAB, Sigma-Aldrich Co.) and 0.28 g of NaOH were solubilized in 480 mL of distilled water at 80 °C under intensive stirring. Then, 5 mL of tetraethyl orthosilicate (TEOS, Sigma-Aldrich Co.) was added dropwise to the clear solution, and the mixture was stirred for 20 h. The synthesized samples were collected by centrifugation at 10 000 rpm for 15 min and washed thoroughly with water and ethanol. Finally, the mixture samples were refluxed three times in the solution containing 500 mL of ethanol and 5 mL of hydrochloric acid at 80 °C for 12 h to remove the surfactant. After collection by centrifugation, MSNs were obtained and dried in the oven at 80 °C for further use.

The surface of MSNs was functionalized with amine groups by treatment with 3-aminopropyltriethoxysilane (APTES, Sigma-Aldrich Co.).[17] Typically, the dried MSNs powder was dispersed in toluene by stirring and sonication, and then, APTES was added to the above solution. The molar ratio of the samples (calculated as MSNs/APTES/toluene) was fixed at 5:1:500, and the suspension was refluxed at 125 °C for 24 h under a nitrogen atmosphere. Finally, MSNs-NH_2 was obtained by centrifugation, washing with toluene and ethanol, and drying under vacuum.

A typical procedure was applied to load DEX into MSNs-NH_2 as in our previously reported procedures.[17] Briefly, 25 mg of DEX was dissolved in a 25 mL mixture of distilled water and ethanol with a concentration of 1 mg/mL. Then, 250 mg of MSNs-NH_2 was soaked in the above DEX solution at room temperature. The suspension was occasionally vacuumed during the stirring under dark condition for 12 h. After that, the mixture was centrifuged at 10 000 rpm for 10 min and washed three times with distilled water. The obtained DEX@MSNs-NH_2 was vacuum-dried at room temperature for 12 h and stored at −20 °C for further use. The supernatant and washing solutions were collected together to determine the DEX loading using a Jasco V530 UV−vis spectrophotometer (Jasco, Japan) at 242 nm.

2.2. Preparation of PLLA/PCL Nanofibrous Scaffold. Three-dimensional (3D) PLLA/PCL nanofibrous scaffold was prepared via the TIPS technique.[13] Typically, PLLA and PCL at the weight ratio of 70:30 were dissolved in tetrahydrofuran (THF) at 60 °C at a concentration of 10% (w/v). Then, the mixture solution was added into the Teflon vial and maintained at −80 °C overnight. Next, the gel was removed from the vial and immersed into cold distilled water (4 °C) for 4 days. The distilled water was changed three times per day. Finally, the 3D PLLA/PCL nanofibrous scaffold was frozen (−20 °C) for at least 6 h and freeze-dried for 24 h.

2.3. Preparation of DEX@MSNs-NH_2/PLLA/PCL Nanofibrous Scaffold. The fabricated PLLA/PCL scaffolds were subsequently used as templates for the deposition of DEX@MSNs-NH_2 nanoparticles by the EPD technique, which was carried out using a CHI600D electrochemistry workstation (Shanghai Chenhua Yi Qi Ltd.) in a conventional three-electrode system. The dried PLLA/PCL scaffold was fixed on the surface of a stainless steel electrode, which served as the working electrode (cathode). A platinum plate electrode and a saturated calomel electrode (SCE) worked, respectively, as the counter electrode (anode) and reference electrode. 100 mg of DEX@MSNs-NH_2 nanoparticles was dispersed in 200 mL of ethanol by stirring and sonication, which was employed as the electrolyte in the EPD method. The setup was immersed in a 25 °C water bath with the stirring speed of 300 rpm. The DEX@MSNs-NH_2 was deposited galvanostatically on the PLLA/PCL scaffold at the desired deposition potential (1, 3, and 5 V) for 30 min. After deposition, the composite scaffold was rinsed with distilled water to remove the residual electrolyte and dried under vacuum for further use.

2.4. Characterization. The surface morphologies of the MSNs-NH_2, PLLA/PCL, and the composite scaffold were observed with a field emission scanning electron microscope (FESEM, Hitachi S-4800,

DOI: 10.1021/acsami.5b11879
ACS Appl. Mater. Interfaces 2016, 8, 4137−4148

Japan). The structure of MSNs-NH_2 was observed by a transmission electron microscope (TEM, Hitachi H-800, Japan) at an operating voltage of 200 kV. To qualitatively analyze the elements distribution in the composite scaffold, the energy dispersive X-ray spectrometry analyses were performed with a Quantax 400 energy dispersive X-ray spectroscope (EDS, Bruker, Germany). The particle size distribution and the polydispersity indexes (PDI) of MSNs-NH_2 were evaluated by dynamic light scattering (DLS) using a BI-200SM multiangle dynamic/static laser scattering instrument (Brookhaven, USA). The zeta potential of the nanoparticles was measured on a Zetasizer Nano ZS apparatus (Malvern, UK).

Nitrogen adsorption−desorption isotherms were measured with a Micromeritics Tristar II analyzer (Micromeritics, USA) at liquid nitrogen temperature under a continuous adsorption condition. Average pore size distributions of MSNs-NH_2 were determined from the desorption branches of isotherms by the Barrett−Joyner−Halenda (BJH) method, and the specific surface area was calculated according to the Brunauer−Emmett−Teller (BET) method. Attenuated total reflection Fourier transform infrared spectroscopy (ATR-FTIR) was performed by a Nicolet-670 FTIR spectrometer (Nicolet-Thermo, USA). All spectra were measured in the wavelength range of 500 to 4000 cm^{-1} with a resolution of 4 cm^{-1}. The thermogravimetric analysis (TGA) was employed to evaluate the weight loss of the samples in nitrogen atmosphere from room temperature to 900 °C at a heating rate of 10 °C min^{-1} using a thermal analyzer (TG 209 F1, Germany). The enzyme degradation rate of the PLLA/PCL scaffold was studied by measuring the weight loss of the scaffold. The scaffold was weighed and incubated in 0.1 mol/L Tris-HCl buffer solution (pH 8.6) containing 50 mg/mL at 37 °C in a thermostatic shaker with the shaking speed of 100 rpm. At preset time intervals, the scaffold was removed and dried under vacuum at room temperature. At last, the weight loss was determined.

2.5. In Vitro DEX Release. The DEX release behavior from the DEX@MSNs-NH_2/PLLA/PCL composite scaffold was investigated in PBS at pH 7.4. Briefly, 50 mg of composite scaffold suspended in 2 mL of PBS was poured in a dialysis bag (cutoff molecular weight 7000 Da), and the bag was soaked in a centrifuge tube filled with 8 mL of PBS. The centrifuge tube was incubated at 37 °C in a thermostatic shaker with the shaking speed of 100 rpm. At selected time intervals, 2 mL of the release medium was taken out and replaced with the same volume of fresh PBS. The collected release medium was determined by a Jasco V530 UV−vis spectrophotometer at a wavelength of 242 nm. The absorbance was converted to its concentration according to the calibration curve of DEX in the same buffer solution. The content of DEX was determined as the average value of three parallel samples.

2.6. Cell Culture. Primary rat bone marrow mesenchymal stem cells (BMSCs) were isolated and expanded on the basis of protocols previously described.[33] Briefly, the bone marrow was obtained from young male Sprague−Dawley (SD) rats (4−6 weeks old, Shanghai Slac laboratory animal co., LTD, China) by cutting off both ends of the femora. Cells were cultured in Dulbecco's Modification of Eagle's Medium/Ham's F-12 (DMEM/F12, Hyclone, China) supplemented with 10% fetal bovine serum (FBS, Gibco, USA), 100 U/mL penicillin, and 100 μg/mL streptomycin (Shanghai Yuanxiang medical equipment Co., Ltd., China) at 37 °C in a humidified CO_2 incubator. The medium was replaced every 3 days during culturing. For all experiments, only early passages (3−5 passages) of BMSCs were used in this study and harvested by using trypsin/EDTA (0.25% w/v and 0.53 mM, respectively) solution and resuspended in the fresh DMEM/F12 medium.

Prior to cell seeding, scaffolds were cut into cylinders with 14 mm diameter and 1 mm thickness so that they fit into 24-well plates, and the mass of each scaffold was 5 mg. Scaffolds were fixed with stainless steel rings, sterilized under UV light for 3 h, and fumigated in 75% ethanol steam overnight.

2.7. Proliferation of BMSCs on the Scaffold. The proliferation of BMSCs cultured on the scaffolds was evaluated by the cell counting kit-8 assay (CCK-8, Beyotime, China) as previously described.[34] Briefly, BMSCs at the density of 5×10^4 cells per well were seeded on the scaffold in 24-well plates and incubated for 3, 7, 10, and 14 d. After a predetermined time point, the culture medium was removed and the cultured cells were washed twice with PBS. Then, 360 μL of the fresh culture medium and 40 μL of CCK-8 solution were added to each well and incubated at 37 °C for another 1 h. An aliquot of 100 μL was transferred to a fresh 96-well microplate, and the absorbance was measured at 450 nm with a microplate reader (MK3, Thermo, USA).

2.8. Morphology of BMSCs on the Scaffold. The morphologies of BMSCs cultured on the scaffold were observed using a scanning electron microscope (SEM, Hitachi TM-1000, Japan) and a confocal laser scanning microscope (CLSM, Carl Zeiss LSM 700, Germany). Briefly, BMSCs were seeded on the scaffold at the density of 5×10^4 cells per well and cultured in a 24-well plate overnight at 37 °C to allow cells to attach. Then, the medium was replaced with the osteogenic medium consisting of DMEM/F12 supplemented with 10% FBS, 100 U/mL penicillin, 100 μg/mL streptomycin, 10 mM sodium β-glycerol phosphate, and L-ascorbic acid (50 μg/mL). After a predetermined time point, the medium was removed and the cultured cells were washed twice with PBS.

For SEM observation, the BMSCs were fixed with 2.5% glutaraldehyde in PBS buffer for 4 h. Then, the fixed samples were dehydrated in an ascending series of ethanol (30%, 50%, 75%, 80%, 90%, and 100%) for 10 min each and dried under vacuum. Afterward, the samples were sputter coated with gold films and observed by SEM at an accelerating voltage of 10 kV.

For CLSM observation, BMSCs were fixed with 4% paraformaldehyde for 15 min at 4 °C. Thereafter, the cells were washed twice with PBS and permeabilized in 0.1% Triton X-100 in PBS for 5 min, followed by blocking with 1% BSA for 20 min. After being washed with PBS, the fixed cells were stained with Alexa Fluor@568 phalloidin solution (165 nM, Invitrogen, China) for 10 min. For nucleus labeling, BMSCs were washed again with PBS and stained with 4′,6-diamidino-2-phenylindole solution (DAPI, 100 nM, Beyotime, China) for 5 min. Then, the samples were washed with PBS and observed by CLSM.

2.9. Alkaline Phosphatase (ALP) Activity. ALP activity as an early osteogenic differentiation marker was measured by using the ALP assay kit (Jiancheng, Nanjing, China). Briefly, 1×10^5 BMSCs were seeded on each scaffold in 24-well plates and cultured in osteogenic medium for 7, 14, and 21 d. At the predetermined time point, the cells were washed with PBS twice to remove the medium and lysed in 300 μL of 0.2% Triton X-100, followed by sonication and centrifugation at 13 000 rpm for 15 min at 4 °C. The supernatant was collected to measure the ALP activity according to the protocol of the ALP assay kit. Meanwhile, the total protein content of each sample was calculated using a BCA protein assay kit (Beyotime, China). The ALP ability was normalized against the total protein content and described as μM/mg total protein.

2.10. Collagen Content. The collagen content of the cells grown on the scaffold was determined by a colorimetric hydroxyproline quantification method.[35] Briefly, at different time points (7, 14, and 21 d), cells were washed with PBS twice and lysed in 300 μL of 0.2% Triton X-100, followed by sonication and centrifugation at 13 000 rpm for 15 min at 4 °C. Then, the lysis solution was assayed by using a hydroxyproline kit (Jiancheng, Nanjing, China) following the manufacturer's instructions.

2.11. Alizarin Red S (ARS) Staining and SEM Observation. To evaluate the mineralization nodules, ARS (Sigma-Aldrich, Germany) staining and SEM observations were performed. Similarly, 1×10^5 BMSCs were seeded on each scaffold in 24-well plates and cultured in osteogenic medium for 14 and 21 d. At the predetermined time point, the cells were washed with PBS and fixed with 2.5% glutaraldehyde in PBS buffer for 4 h at 4 °C. Then, the cells were washed with distilled water and stained with 20 mg/mL ARS (pH 4.2) for 30 min at room temperature. After the cells were washed several times with distilled water, the ARS staining was imaged using a camera (Canon EOS 550D). For quantification of the staining of each sample, 10% acetic acid was added to each sample and incubated overnight. Then, the solution was collected and centrifuged for 15 min at 13 000 rpm. The supernatant was extracted and neutralized with 10% ammonium hydroxide. 100 μL of the mixture solution was transferred to a 96-well

DOI: 10.1021/acsami.5b11879
ACS Appl. Mater. Interfaces 2016, 8, 4137−4148

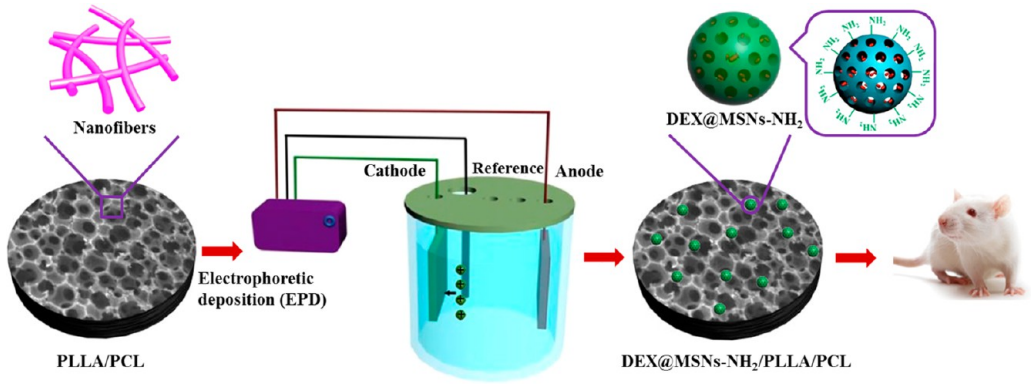

Figure 1. Schematic illustration for the process of fabrication of the DEX@MSNs-NH_2/PLLA/PCL composite scaffold.

plate, and the optical density (OD) value was recorded at 405 nm using a microplate reader.

The mineralization nodules of the cells were also observed by environmental scanning electron microscopy (ESEM, Quanta-250, Czech) after incubation for 14 d, and the compositional analysis was measured by energy diffraction X-ray (EDS, AZtec X-Max 20, England).

2.12. Osteocalcin (OCN) Staining. OCN, a noncollagenous protein, affects the mineralization and the calcium ion homeostasis of BMSCs.[36] At the predetermined time points (14 and 21 d), BMSCs were washed with PBS and fixed with 10% formalin solution for 20 min at 4 °C, then permeabilized with 0.1% Triton X-100 solution for 5 min, and nonspecific binding blocked with 10% normal donkey serum for 30 min. Cells on the scaffolds were incubated overnight at 4 °C with the primary antibody (mouse antihuman/rat osteocalcin monoclonal antibody, 10 μg/mL, R&D, USA). After that, cells were washed three times with PBS and incubated for 1 h with donkey antimouse IgG secondary antibody conjugated to fluorochrome NL557 (5 μg/mL, R&D, USA). Finally, the cell nuclei were stained by DAPI and observed by CLSM. The intensity of OCN was measured by the computerized image analysis software Image-Pro Plus for five randomly selected fields of the CLSM images.

2.13. Animal Model. All animal experiments were performed in compliance with the Institutional Animal Care and Use Committees (IACUC) guidelines. Eight-week-old male SD rats (Shanghai Slac laboratory animal co., LTD, China) were used and randomly assigned to three different treatment groups: (1) empty defect control (n = 8), (2) PLLA/PCL scaffold (n = 8), and (3) DEX@MSNs-NH_2/PLLA/PCL (n = 8).

The scaffolds were prepared and treated with UV light for sterilization prior to implantation. For the calvarial bone defects, the rats were first under general anesthesia. Then, a 2.0−2.5 cm sagittal incision was made on the scalp, and the cranium was exposed by blunt dissection. For each animal, the calvarial bone defect was created on one side of the skull by a 6 mm diameter trephine bur under low speed drilling with continuous cool saline irrigation. The prepared scaffolds (6 mm diameter, 2 mm thickness) were implanted into the defects, and the blank groups were left untreated. In all animals, following the 0.9% saline rinse, the incision was closed in layers using the sutures. After operation, the rats were able to function normally.

2.14. Microcomputed Tomography (micro-CT) Measurement. In order to evaluate the osteogenesis in vivo of the different groups, the scan was acquired with a high-resolution Triumph small animal microcomputed tomography (micro-CT) scanner (Gamma Medica, USA) at 4, 8, 12, and 24 W. After scanning, the initial scans were collected and the 3D images were reconstructed using the GEHC microview software (GE Healthcare BioSciences, Chalfont St. Giles, UK).

2.15. Histology Analysis. After micro-CT analysis, the rats of different groups were sacrificed at predetermined time points (12 and 24 W). The calvaria encompassing the parietal defects were cut from the skulls and fixed in 4% paraformaldehyde overnight, dehydrated in an ascending series of ethanol (70%, 75%, 80%, 85%, 90%, 95%, and 100%) for 24 h each, and embedded in poly(methyl methacrylate) (PMMA, Sinopharm Chemical Reagent Co., Ltd.). The sections of undecalcified specimens were assigned for histological analysis. The sagittal sections representing the central area of the defect were cut into 150 μm thick sections using a saw microtome (Leica SP1600, Hamburg, Germany) and polished to a final thickness of approximately 40 μm.

For histological analysis, the sections were treated with hematoxylin and eosin (H&E), Toluidine blue (T-blue), and Goldner's trichrome staining to identify new bone formation. To examine the osteogenesis, the sections were stained for ALP following the manufacturer's instructions (Jiancheng, Nanjing). Then, the stained sections were visualized under a light microscope (Laica, Italy).

2.16. Statistical Analysis. All the data were expressed as means ± standard deviations (SD) from three independent experiments. Statistical analysis was performed using the one-way analysis of variance (one-way ANOVA) and the Scheffe's post hoc test. The criteria for statistical significance were as follows: *, $P < 0.05$; **, $P < 0.01$.

3. RESULTS AND DISCUSSION

The brief fabrication process is presented in Figure 1. MSNs were synthesized as previously reported and modified with amine groups by treatment with 3-aminopropyltriethoxysilane (APTES). Then, DEX was loaded into MSNs-NH_2, and the loading efficiency was calculated to be 8.09%. After that, the prepared DEX@MSNs-NH_2 was deposited on the 3D PLLA/PCL scaffold by the EPD technique, constructing the DEX@MSNs-NH_2/PLLA/PCL composite scaffold.

3.1. Characterization of MSNs-NH_2. The structural and textural characterizations of the as-prepared MSNs-NH_2 are shown in Figure S1. It can be found that MSNs-NH_2 showed an elliptic morphology, uniform particle size, and a relatively narrow particle size distribution, with the mean hydrodynamic size of 318.8 nm measured by DLS (Figure S1A,D). The polydispersity index (PDI) of nanoparticles was 0.27, indicating MSNs-NH_2 particles exhibited good dispersity in ethanol. The zeta potential of MSNs-NH_2 is 7.72 ± 0.40 mV due to the presence of amino groups, which would favor the deposition of DEX@MSNs-NH_2 onto the scaffold fixed on the cathode. A typical TEM image (Figure S1B) shows that the MSNs-NH_2 owns a highly ordered mesoporous structure. The nitrogen adsorption−desorption isotherms and pore size distribution data of MSNs-NH_2 are shown in Figure S1C, which indicated the characteristics of mesoporous materials.[29] The BET surface area and the BJH pore diameter of MSNs-NH_2 were 972.58 m^2/g and 2.97 nm, respectively, which offers a large internal volume for drug loading.

DOI: 10.1021/acsami.5b11879
ACS Appl. Mater. Interfaces 2016, 8, 4137−4148

3.2. Physical Properties of DEX@MSNs-NH_2/PLLA/PCL.

Figure 2 shows the SEM micrographs of the PLLA/PCL and DEX@MSNs-NH_2/PLLA/PCL produced at the varied deposition potential (1, 3, and 5 V) for 30 min. The PLLA/PCL scaffold macrocosmically exhibited a 3D porous network structure with interconnected micropores and microscopically showed continuous nanofibrous architecture (Figure 2A and inset). This could be attributed to PLLA facilitating the gelation of PLLA/PCL mixtures and phase separation happening between the two polymers and then resulting in the formation of a nanofibrous structure via the TIPS technique.[13,37] The pore diameter of the scaffold was approximately 15.66 μm. After deposition, DEX@MSNs-NH_2 particles were observed on the walls and inside of the pores of the scaffold, as shown in Figure 2B–D. Specifically, in the case of low deposition potential (1 V), few nanoparticles were deposited on the walls of pores. With the deposition potential increasing to 3 V, more particles were observed on the scaffold, and the porous structure was still maintained. However, when the voltage was increased to 5 V, the scaffold was fully covered with DEX@MSNs-NH_2 particles, so that the porous structure of the scaffold was hidden, which is not beneficial for the cell ingrowth. From the EDS elemental mapping and EDS spectra for Si, C, and O of the composite scaffold, it was found that Si, C, and O were the most abundant elements and distributed uniformly (Figure S2). The result indicated that DEX@MSNs-NH_2 particles were uniformly deposited on the scaffold both outside and inside of the pores and the porous structure was still intact. Therefore, the composite scaffold produced at 3 V was selected for subsequent drug release, in in vitro and in vivo experiments.

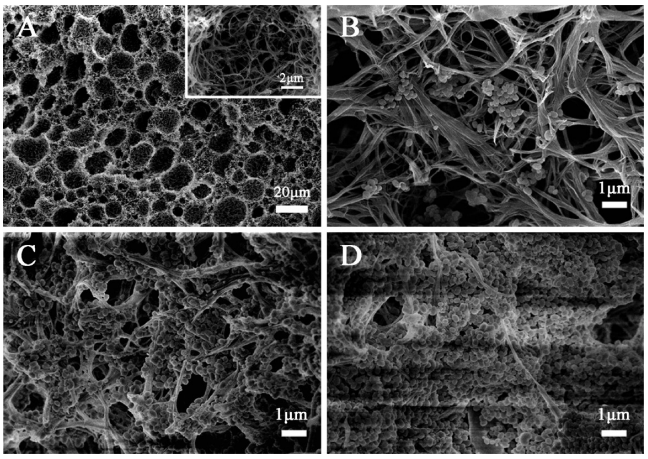

Figure 2. FESEM images of (A) PLLA/PCL (inset is the microstructure) and DEX@MSNs-NH_2/PLLA/PCL composite scaffold prepared at varied deposition potential: (B) 1 V, (C) 3 V, and (D) 5 V.

The chemical structures of the DEX, MSNs, MSN-NH_2, PLLA/PCL, and DEX@MSNs-NH_2/PLLA/PCL composite scaffold were analyzed using ATR-FTIR (Figure S3A). The characteristic peaks of DEX at 900 and 1650 cm^{-1} were not observed in the spectrum of DEX@MSNs-NH_2 /PLLA/PCL, which confirmed that there was no DEX on the surface of the composite scaffold. From the spectrum of MSNs, the peaks at 795 and 953 cm^{-1} can be assigned to the Si–O–Si and Si–OH stretching vibrations of MSNs, and the broad peak in the range of 3750–3000 cm^{-1} is associated with the stretching vibration of the Si–OH group.[38,39] Moreover, the incorporation of amino groups on the MSNs surface was also qualitatively confirmed by the FTIR spectrum of MSNs-NH_2. A new adsorption peak was observed at 1555 cm^{-1}, which could be assigned to the N–H asymmetric bending vibration.[39] The PLLA/PCL scaffold showed the absorption peaks at 1758 and 2944 cm^{-1} corresponding to the C=O and C–H stretching vibration in PLLA and PCL.[13] However, the peak of the Si–OH stretching vibration at 953 cm^{-1} was also shown in the spectrum of DEX@MSNs-NH_2/PLLA/PCL, confirming that DEX@MSNs-NH_2 was successfully deposited on the PLLA/PCL scaffold.

Thermal analysis of the MSNs-NH_2, DEX@MSNs-NH_2, PLLA/PCL, and DEX@MSNs-NH_2/PLLA/PCL was performed by using TGA. As shown in Figure S3B, a weight decrease in the TGA curves for MSNs-NH_2 and DEX@MSNs-NH_2 before 100 °C could be due to the vaporization of water in the particles. From the curves of PLLA/PCL and DEX@MSNs-NH_2/PLLA/PCL in Figure S3B, the weight decreased rapidly from approximately 250 to 400 °C, which can be attributed to the strong decomposition of PLLA and DEX. The weight percentages of residual MSNs were 80.26%, 68.79%, and 3.54% for MSNs-NH_2, DEX@MSNs-NH_2, and DEX@MSNs-NH_2/PLLA/PCL, respectively. As a result, the DEX content in the MSN-NH_2 can be calculated to be 8.31%, which was almost consistent with the DEX loading efficiency in MSNs-NH_2

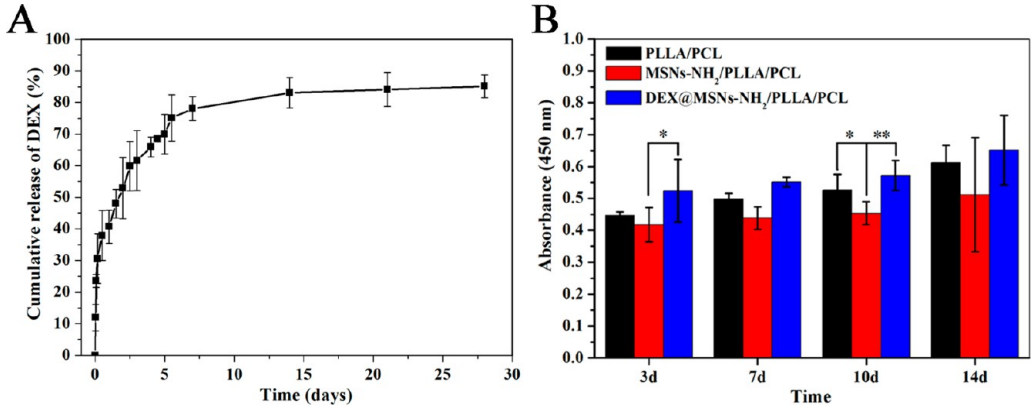

Figure 3. (A) The cumulative DEX release profile from DEX@MSNs-NH_2/PLLA/PCL composite scaffold. (B) Cell viability of BMSCs cultured on the PLLA/PCL, MSNs-NH2/PLLA/PCL, and DEX@MSNs-NH2/PLLA/PCL scaffolds for 3, 7, 10, and 14 d. The significant difference between groups is indicated (*, $P < 0.05$; **, $P < 0.01$).

DOI: 10.1021/acsami.5b11879
ACS Appl. Mater. Interfaces 2016, 8, 4137–4148

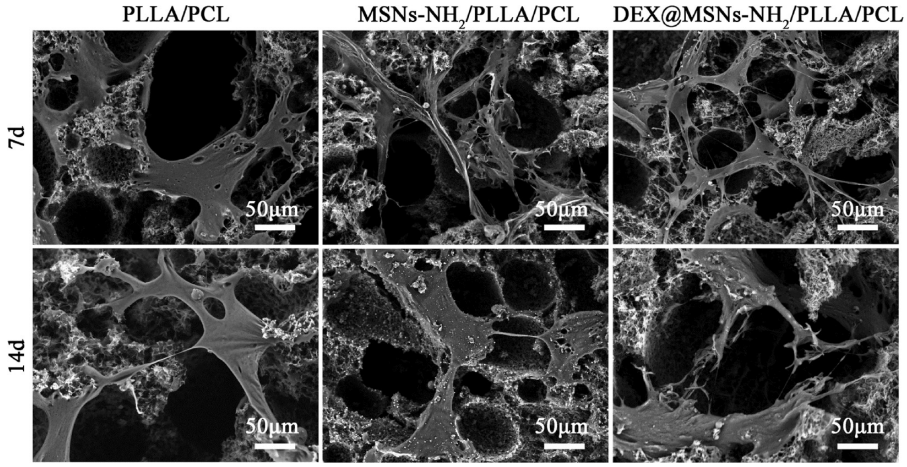

Figure 4. SEM micrographs of BMSCs cultured on the PLLA/PCL, MSNs-NH_2/PLLA/PCL, and DEX@MSNs-NH_2/PLLA/PCL scaffolds for 7 and 14 d.

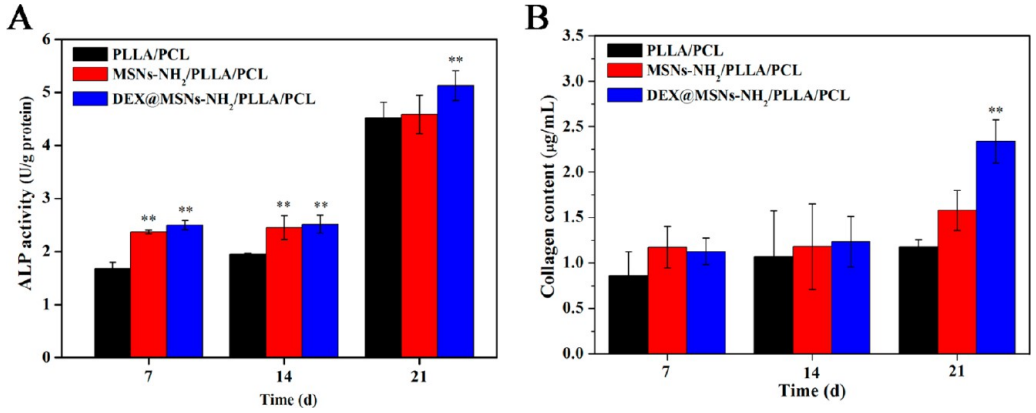

Figure 5. (A) In vitro alkaline phosphatase (ALP) activity and (B) collagen content of BMSCs cultured on the PLLA/PCL, MSNs-NH_2/PLLA/PCL, and DEX@MSNs-NH_2/PLLA/PCL scaffolds for 7, 14, and 21 d. The significant difference between groups is indicated (**, $P < 0.01$).

measured by UV−vis spectra. Consequently, the DEX content in the DEX@MSNs-NH_2/PLLA/PCL was approximately 0.078 μg/mg.

The release kinetics of DEX was shown in Figure 3A. The release of DEX from the DEX@MSNs-NH_2/PLLA/PCL composite scaffold exhibited an initial burst release followed by a constant release during 28 d of incubation. Specifically, approximately 12% of the initially loaded DEX was released from the composite scaffold after the first 1 h and around 40% after the first day, followed by a slow release up to 80% during the subsequent 4 weeks.

The enzyme degradation rate of the PLLA/PCL scaffold was shown in Figure S3C. The PLLA/PCL scaffold could lose approximately 46.2% of its weight after incubation in Tris-HCl with proteinase K for 16 d.

3.3. Osteogenesis Evaluations in Vitro. *Cell Viability Evaluation.* To investigate the cell viability of PLLA/PCL, MSNs-NH_2/PLLA/PCL, and DEX@MSNs-NH_2/PLLA/PCL, BMSCs were cultured on the scaffolds and the cell viability was evaluated by using a standard CCK-8 assay. As shown in Figure 3B, the result showed that the cell number gradually increased with the culture period from 3 to 14 d for all the scaffolds. For a 14 d incubation, it is obviously observed that all the scaffolds did not show statistical differences in cell viability, indicating the deposition of MSNs-NH_2 on the scaffolds will not cause any cytotoxicity compared to the pure scaffold. Therefore, the prepared scaffold has good biocompatibility, which is kindly used in the further study in vivo.

The adhesion and proliferation of BMSCs after incubation on the scaffold for 7 and 14 d were studied by SEM and CLSM. As shown in Figure 4, BMSCs seeded on the scaffolds spread around the pore with elongated shape and a few thin pseudopodia after 7 d. With the incubation being prolonged, BMSCs became bigger in size and showed more outstretched filopodia-like extensions, which was significantly obvious on the DEX@MSNs-NH_2/PLLA/PCL scaffold. It is notable that BMSCs cultured on the DEX@MSNs-NH_2/PLLA/PCL scaffold spread better and had more filopodia to grow toward the inside of the pores than those on PLLA/PCL and MSNs-NH_2/PLLA/PCL.[40] These similar morphologies of BMSCs can be further confirmed by CLSM images after a 14 d incubation (Figure S4), in which the blue fluorescence of the DAPI-stained cell nuclei and red fluorescence of the Alexa Fluor@568 phalloidin-stained F-actin were clearly observed. Obviously, BMSCs grew on the DEX@MSNs-NH_2/PLLA/PCL scaffold spread well.

ALP Activity and Collagen Content. ALP, a cell membrane bound enzyme, guarantees that BMSCs move toward the osteoplastic cell, so ALP activity is an early marker and plays an important role in osteogenic differentiation of BMSCs.[35,41] Moreover, many studies reported that DEX could induce osteoblast differentiation and bone formation of BMSCs.[29,30,42]

DOI: 10.1021/acsami.5b11879
ACS Appl. Mater. Interfaces 2016, 8, 4137−4148

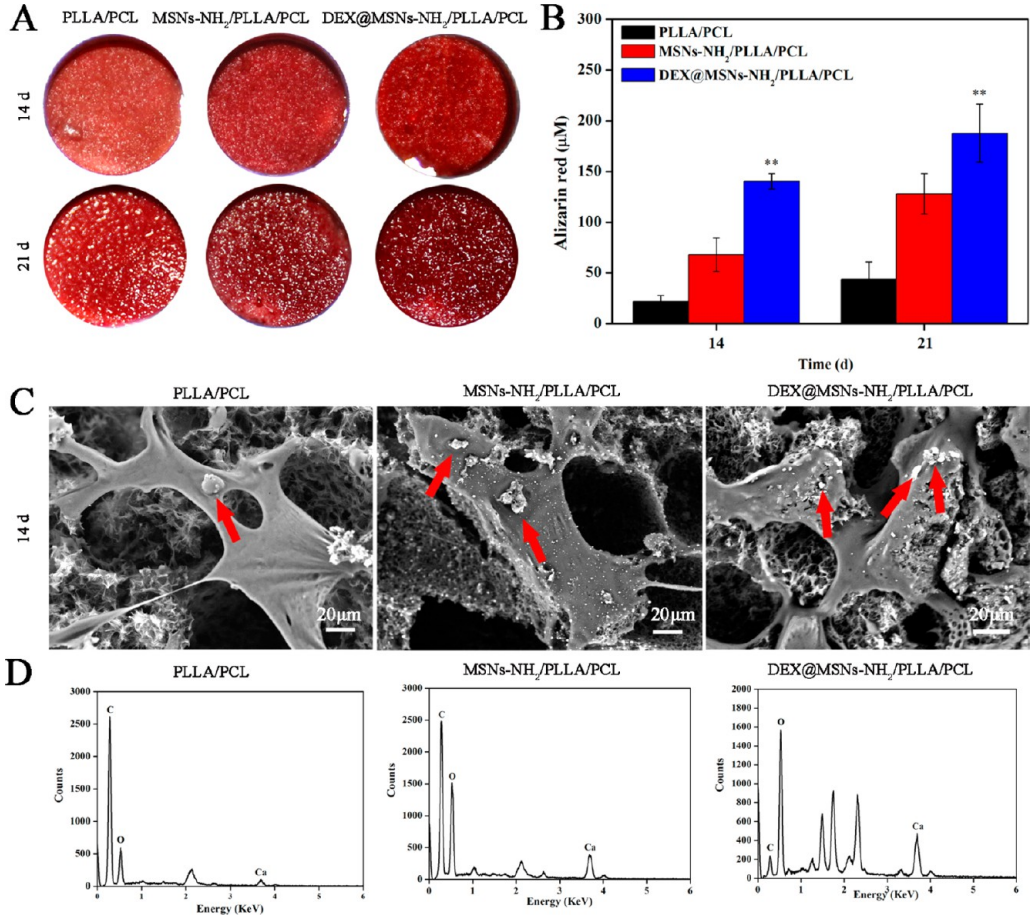

Figure 6. Evaluations of mineralized matrix produced by BMSCs after incubation on the PLLA/PCL, MSNs-NH_2/PLLA/PCL, and DEX@MSNs-NH_2/PLLA/PCL for 14 and 21 d. (A) Digital photos of different samples after staining with Alizarin Red S (ARS). (B) The production of mineralized matrix determined by quantifying the amount of Alizarin Red S that stained the mineralized matrix. The significant difference between groups is indicated (**, $P < 0.01$). (C) SEM images of the calcium mineral nodules deposited by BMSCs after incubation for 14 d. (D) EDS analysis corresponding to the SEM images of calcium mineral nodules deposition.

Herein, the effect of DEX released from the DEX@MSNs-NH_2/PLLA/PCL scaffold on BMSCs after 7, 14, and 21 d of culture was investigated (Figure 5A), and the results for PLLA/PCL and MSNs-NH_2/PLLA/PCL were also investigated for comparison. It can be observed that the ALP activity of BMSCs on the MSNs-NH_2/PLLA/PCL and DEX@MSNs-NH_2/PLLA/PCL was significantly stronger than that on the PLLA/PCL scaffold ($P < 0.01$) for 7 and 14 d, suggesting the introduction of the particles could trigger the upregulation of ALP in the early stage. However, after 21 d of culture, the ALP activity of BMSCs cultured on the DEX@MSNs-NH_2/PLLA/PCL scaffold was 5.13 ± 0.28 U/g proteins, which is significantly higher than 4.52 ± 0.29 U/g proteins for PLLA/PCL and 4.58 ± 0.36 U/g proteins for the MSNs-NH_2/PLLA/PCL scaffold ($P < 0.01$). The results could be attributed to the effect of the DEX released from the scaffold.

In addition to the ALP ability, collagen synthesis is another osteoblast-associated marker.[35,43] BMSCs grown and differentiated on the scaffolds also produced collagen, the major extracellular matrix of bone, as shown in Figure 5B. At the early stage (7 and 14 d), BMSCs produced a similar collagen content on all the scaffolds, which was only affected by the osteogenic medium. Furthermore, with the incubation time increasing to 21 d, a significant greater degree of collagen (2.34 ± 0.24 μg/mL) was produced by BMSCs grown on the DEX@MSNs-NH_2/PLLA/PCL scaffold compared to BMSCs on the scaffold without the presence of DEX (1.18 ± 0.08 μg/mL for PLLA/PCL and 1.58 ± 0.22 μg/mL for MSNs-NH_2/PLLA/PCL, $P < 0.01$), which has a similar tendency with the ALP ability, further indicating the released DEX had the promoting effects on the differentiation of BMSCs.

In Vitro Mineralization. Mineralized matrix formation was examined by Alizarin Red S staining and SEM images, which identifies calcium deposition, and the extent of calcium deposition was quantified by extracting the dye from the stained monolayer and identified by EDS, as shown in Figure 6. When BMSCs were cultured for 14 and 21 d, the calcium deposition was stained with red spots (Figure 6A). The color intensity of the DEX@MSNs-NH_2/PLLA/PCL scaffold was obviously stronger than the other two scaffolds, which was in agreement with the SEM images that more calcium nodules were observed on the DEX@MSNs-NH_2/PLLA/PCL scaffold (Figure 6C). Furthermore, the EDS corresponding to the SEM images confirmed the presence of calcium deposition on the scaffolds (Figure 6D). Qualitatively, the Alizarin Red S reflecting the amount of the calcium deposition was statistically significantly higher on the DEX@MSNs-NH_2/PLLA/PCL scaffold than that on the PLLA/PCL and MSNs-NH_2/PLLA/PCL scaffolds ($P < 0.01$, Figure 6B). These observations indicated that DEX released from the DEX@MSNs-NH_2/

DOI: 10.1021/acsami.5b11879
ACS Appl. Mater. Interfaces 2016, 8, 4137−4148

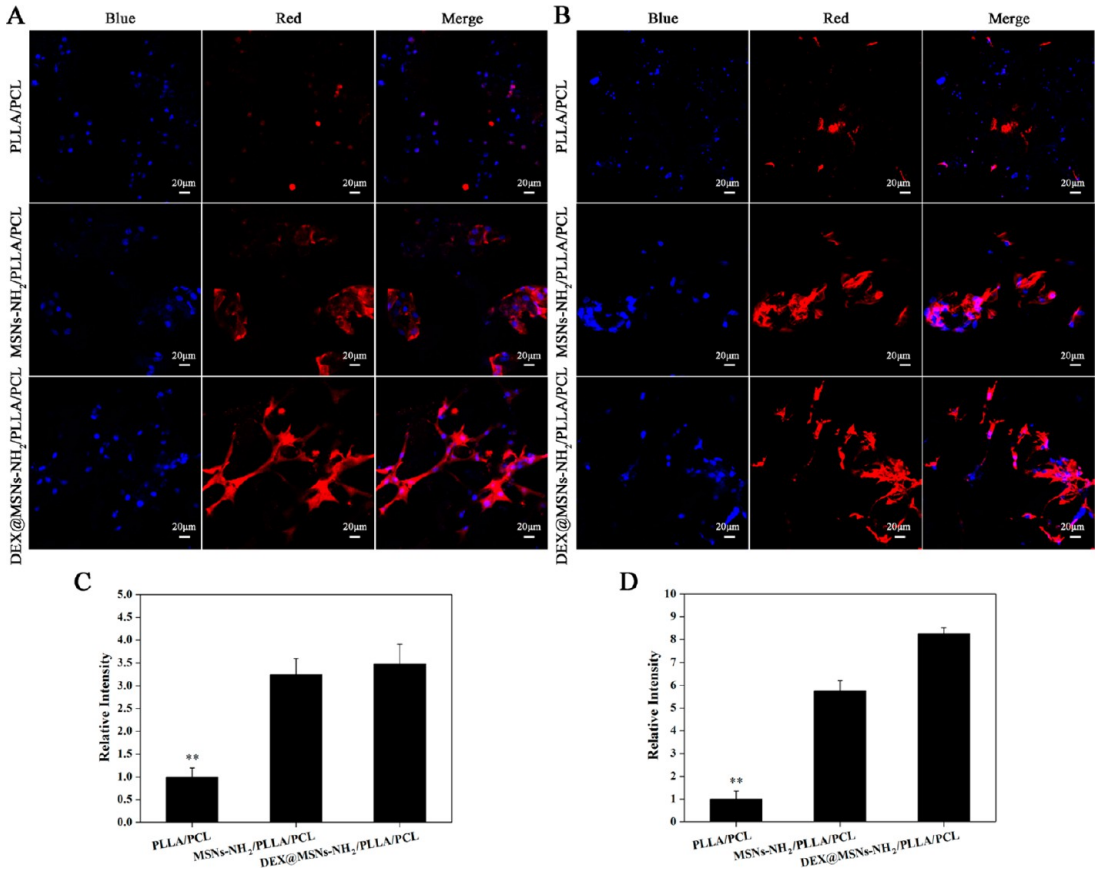

Figure 7. OCN staining of BMSCs cultured on the PLLA/PCL, MSNs-NH_2/PLLA/PCL, and DEX@MSNs-NH_2/PLLA/PCL scaffolds and the corresponding quantitative analysis for (A, C) 14 d and (B, D) 21 d. The significant difference between groups is indicated (**, $P < 0.01$).

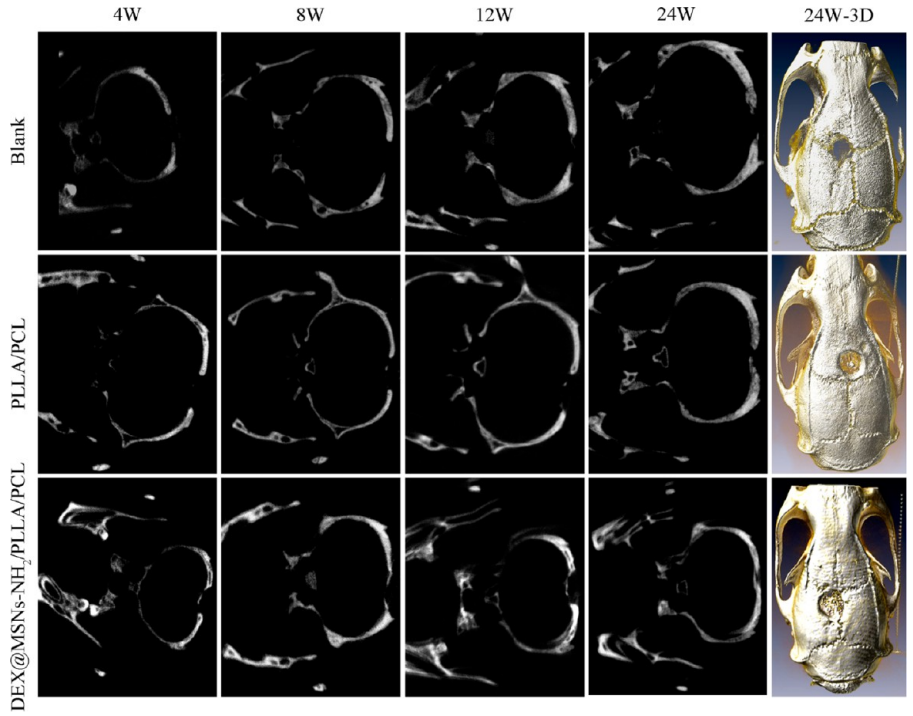

Figure 8. Micro-CT evaluation of SD rats calvarial bone defects. Images of plain micro-CT scanning at 4, 8, 12, and 24 W (left) and 3D micro-CT reconstruction after 24 W (right) implantation of the blank and the PLLA/PCL and DEX@MSNs-NH_2/PLLA/PCL scaffolds.

PLLA/PCL scaffold could induce the matrix mineralization that occurs along the differentiation of BMSCs.

OCN Immunofluorescence. OCN, as a specific marker for the late stage of osteogenic differentiation, plays a key role in

DOI: 10.1021/acsami.5b11879
ACS Appl. Mater. Interfaces 2016, 8, 4137−4148

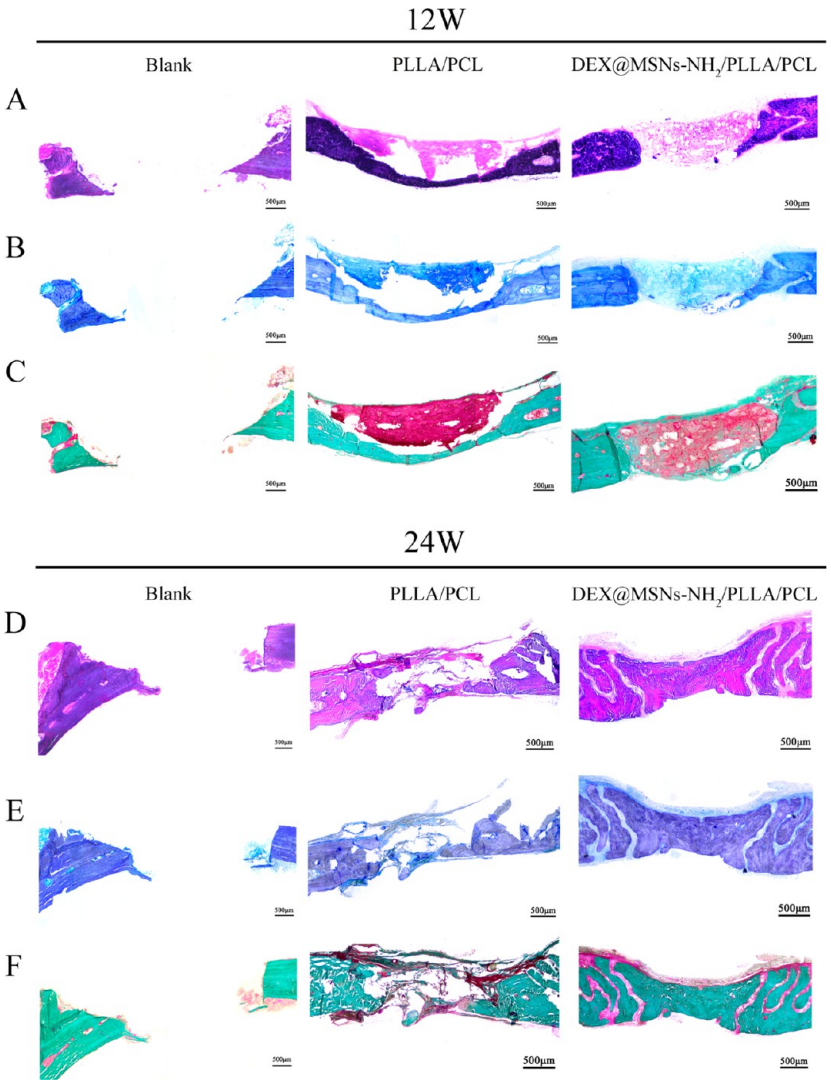

Figure 9. (A, D) H&E staining analysis, (B, E) T-blue staining analysis, and (C, F) Goldner's staining analysis of SD rats calvarial bone defects after 12 and 24 W implantation of the blank and the PLLA/PCL and DEX@MSNs-NH_2/PLLA/PCL scaffolds.

regulating bone formation and mineralization.[44] As shown in Figure 7, the OCN expression of BMSCs cultured on the scaffolds (14 and 21 d) was assessed by immunofluorescence and the intensity of OCN was also measured from the CLSM images. It was obviously seen that the red fluorescence on the MSNs-NH_2/PLLA/PCL and DEX@MSNs-NH_2/PLLA/PCL scaffolds was enhanced compared with the blank scaffold at the same time point, indicating that the expression of OCN was significantly higher on the MSNs-NH_2/PLLA/PCL and DEX@MSNs-NH_2/PLLA/PCL scaffolds, which was also identified by the data of the relative intensity ($P < 0.01$). Furthermore, the fluorescence intensity on the MSNs-NH_2/PLLA/PCL (5.75 ± 0.46) and DEX@MSNs-NH_2/PLLA/PCL (8.26 ± 0.25) scaffolds at 21 d was approximately two times higher than that at 14 d (3.24 ± 0.35 for MSNs-NH_2/PLLA/PCL and 3.48 ± 0.43 for DEX@MSNs-NH_2/PLLA/PCL), which inferred that the higher degree of OCN at 21 d inflected the stronger ability of osteogenic differentiation.

3.4. Evaluations of Orthotopic Bone Formation. *Micro-CT Analysis.* The effects of the implanted scaffold on the in vivo calvarial bone defects were evaluated by imaging with micro-CT at 4, 8, 12, and 24 W (Figure 8). The reconstructed 3D micro-CT images at 24 W after implantation directly indicated the bone formation. As for the blank group (without scaffold), the sagittal view demonstrated that the margin of the defects was becoming irregular from 4 to 24 W, and the reconstructed 3D micro-CT images showed that little high density area was observed, which indicated that few bone defects were repaired. However, more high density spots were observed after implanting the PLLA/PCL and DEX@MSNs-NH_2/PLLA/PCL scaffolds. Specially, the reconstructed 3D micro-CT images of the DEX@MSNs-NH_2/PLLA/PCL group suggested the substantial bone healing at 24 W, whereas the bone repair was slower and inferior in the PLLA/PCL group. This phenomenon indicated that the released DEX exerted functions effectively, which was in agreement with the results in vitro.

Calvarial Bone Formation Evaluated by Histology. New bone formation in calvarial defects was confirmed histologically with H&E, T-blue, and Goldner's trichrome staining (Figure 9). From the H&E, T-blue, and Goldner's trichrome staining, there is little bone formation after 12 and 24 W post-implantation in the blank group, which could be attributed to there being no scaffold in the defects to support the cell adhesion and migration. From H&E staining, there were no obvious inflammatory response and rejection reaction in the defect sites treated with PLLA/PCL and DEX@MSNs-NH_2/

DOI: 10.1021/acsami.5b11879
ACS Appl. Mater. Interfaces 2016, 8, 4137−4148

PLLA/PCL (Figure 9A,D), indicating that PLLA and PCL have good biocompatibility. As shown in Figure 9A,D, the scaffold has degraded completely and the defect began to heal after 12 W implantation. In addition, the rate of healing of the defect treated with PLLA/PCL was slower than that with DEX@MSNs-NH_2/PLLA/PCL scaffold, and the defect site treated with the latter scaffold was filled with abundant soft tissues at 24 W (Figure 9D), which indicated that DEX could promote the defect repair.

To examine the new bone formation, the sections were also stained by T-blue and Goldner's trichrome. Light blue and pink osteoid were obviously observed at the defect sites after 12 W implantation in Figure 9B,C, which suggested that the cartilage matrices were newly formed.[45,46] After 24 W implantation, only part of the osteoid had mineralized with the PLLA/PCL scaffold, whereas almost all the cartilage matrices had mineralized and formed mature bone tissues with the DEX@MSNs-NH_2/PLLA/PCL scaffold (Figure 9E,F). These results further confirmed that DEX@MSNs-NH_2/PLLA/PCL could not only support the BMSCs adhesion and migration but also induce the BMSCs to differentiation.

ALP staining of the sections after 12 and 24 W post-implantation was performed by using the calcium cobalt method, and the stained images were shown in Figure S5. A similar phenomenon in the blank group occurred with other staining. At 12 W, the defect sites were light red in the PLLA/PCL and DEX@MSNs-NH_2/PLLA/PCL group, which indicated ALP activity was strong in the early period. With the implantation time being prolonged to 24 W, ALP activity became weaker and the defect treated with DEX@MSNs-NH_2/PLLA/PCL was almost healed at 24 W. These results showed that the healing rate of the calvarial defect with the DEX@MSNs-NH_2/PLLA/PCL scaffold is faster than that with the PLLA/PCL scaffold.

4. CONCLUSION

In this study, the DEX loaded MSNs-NH_2 nanoparticles were uniformly deposited onto the 3D PLLA/PCL scaffold by the EPD technique, thus fabricating the DEX@MSNs-NH_2/PLLA/PCL composite scaffold for bone tissue engineering. The DEX@MSNs-NH_2/PLLA/PCL scaffold still keeps the porous and nanofibrous structure, which was beneficial for cell adhesion and ingrowth. The DEX-loading capability of the composite scaffold is determined to be 0.078 μg/mg, and DEX released from the composite scaffold in a sustained release profile. The cell viability studies showed that the composite scaffold possesses good biocompatibility to support the proliferation of BMSCs. More importantly, the DEX@MSNs-NH_2/PLLA/PCL composite scaffold presented a significantly enhanced osteogenic differentiation and mineralization compared with the PLLA/PCL or MSNs-NH_2/PLLA/PCL composite scaffolds. Furthermore, the in vivo results indicated the DEX@MSNs-NH_2/PLLA/PCL composite scaffold significantly enhanced the calvarial bone healing after 24 W postimplantation when compared with two other scaffolds. Therefore, this study provides a fast and convenient method to obtain a microcarriers-incorporated composite scaffold, and the prepared 3D DEX@MSNs-NH_2/PLLA/PCL scaffold is of great potential for bone regeneration.

ASSOCIATED CONTENT

Supporting Information

The Supporting Information is available free of charge on the ACS Publications website at DOI: 10.1021/acsami.5b11879.

Characterization of MSNs-NH_2, EDS elemental mapping and EDS analysis for Si, C, and O in the composite scaffold under 3 V for 1800 s at 25 °C, characterization of the PLLA/PCL and DEX@MSNs-NH_2/PLLA/PCL scaffolds, confocal laser scanning microscopy (CLSM) images of BMSCs cultured on the PLLA/PCL, MSNs-NH_2/PLLA/PCL, and DEX@MSNs-NH_2/PLLA/PCL scaffolds, and ALP staining analysis of SD rats calvarial bone defects after 12 and 24 W implantation of the blank and the PLLA/PCL and DEX@MSNs-NH_2/PLLA/PCL scaffolds. (PDF)

AUTHOR INFORMATION

Corresponding Author

*Tel./Fax: +86 21 6779 2742. E-mail: hcl@dhu.edu.cn.

Notes

The authors declare no competing financial interest.

ACKNOWLEDGMENTS

This study was financially supported by the National Natural Science Foundation of China (31271028, 31570984), Innovation Program of Shanghai Municipal Education Commission (13ZZ051), International Cooperation Fund of the Science and Technology Commission of Shanghai Municipality (15540723400), Open Foundation of State Key Laboratory for Modification of Chemical Fibers and Polymer Materials (LK1416), and Chinese Universities Scientific Fund (CUSF-DH-D-2013008).

REFERENCES

(1) Cui, Y. Y.; Han, X. G.; Wang, J. Y.; Song, Q. S.; Tan, J.; Fu, X.; Xu, Y. S.; Song, C. L. Calvarial Defect Healing by Recruitment of Autogenous Osteogenic Stem Cells Using Locally Applied Simvastatin. *Biomaterials* **2013**, *34*, 9373−9380.

(2) Kasten, P.; Luginbuhl, R.; van Griensven, M.; Barkhausen, T.; Krettek, C.; Bohner, M.; Bosch, U. Comparison of Human Bone Marrow Stromal Cells Seeded on Calcium-Deficient Hydroxyapatite, β-Tricalcium Phosphate and Demineralized Bone Matrix. *Biomaterials* **2003**, *24*, 2593−2603.

(3) Crane, G. M.; Ishaug, S. L.; Mikos, A. G. Bone Tissue Engineering. *Nat. Med.* **1995**, *1*, 1322−1324.

(4) He, C. L.; Nie, W.; Feng, W. Engineering of Biomimetic Nanofibrous Matrices for Drug Delivery and Tissue Engineering. *J. Mater. Chem. B* **2014**, *2*, 7828−7848.

(5) Ma, P. X. Biomimetic Materials for Tissue Engineering. *Adv. Drug Delivery Rev.* **2008**, *60*, 184−198.

(6) Liao, J. F.; Qu, Y.; Chu, B. Y.; Zhang, X. N.; Qian, Z. Y. Biodegradable CSMA/PECA/Graphene Porous Hybrid Scaffold for Cartilage Tissue Engineering. *Sci. Rep.* **2015**, *5*, 9879.

(7) Liao, J. F.; Shi, K.; Ding, Q. X.; Qu, Y.; Luo, F.; Qian, Z. Y. Recent Developments in Scaffold-Guided Cartilage Tissue Regeneration. *J. Biomed. Nanotechnol.* **2014**, *10*, 3085−3104.

(8) Fu, S. Z.; Ni, P. Y.; Wang, B. Y.; Chu, B. Y.; Peng, J. R.; Zheng, L.; Zhao, X.; Luo, F.; Wei, Y. Q.; Qian, Z. Y. In Vivo Biocompatibility and Osteogenesis of Electrospun Poly(ε-Caprolactone)-Poly(Ethylene Glycol)-Poly(ε-Caprolactone)/Nano-Hydroxyapatite Composite Scaffold. *Biomaterials* **2012**, *33*, 8363−8371.

(9) Richardson, T. P.; Peters, M. C.; Ennett, A. B.; Mooney, D. J. Polymeric System for Dual Growth Factor Delivery. *Nat. Biotechnol.* **2001**, *19*, 1029−1034.

DOI: 10.1021/acsami.5b11879
ACS Appl. Mater. Interfaces 2016, 8, 4137−4148

(10) Stevens, M. M.; George, J. H. Exploring and Engineering the Cell Surface Interface. *Science* **2005**, *310*, 1135−1138.
(11) He, C. L.; Huang, Z. M.; Han, X. J. Fabrication of Drug-loaded Electrospun Aligned Fibrous Threads for Suture Applications. *J. Biomed. Mater. Res., Part A* **2009**, *89A*, 80−95.
(12) Zhang, Z. P.; Hu, J.; Ma, P. X. Nanofiber-Based Delivery of Bioactive Agents and Stem Cells to Bone Sites. *Adv. Drug Delivery Rev.* **2012**, *64*, 1129−1141.
(13) Wang, W. Z.; Hu, J. W.; He, C. L.; Nie, W.; Feng, W.; Qiu, K. X.; Zhou, X. J.; Gao, Y.; Wang, G. Q. Heparinized PLLA/PLCL Nanofibrous Scaffold for Potential Engineering of Small-Diameter Blood Vessel: Tunable Elasticity and Anticoagulation Property. *J. Biomed. Mater. Res., Part A* **2015**, *103*, 1784−1797.
(14) Wei, G. B.; Jin, Q. M.; Giannobile, W. V.; Ma, P. X. Nano-Fibrous Scaffold for Controlled Delivery of Recombinant Human PDGF-BB. *J. Controlled Release* **2006**, *112*, 103−110.
(15) Vallet-Regi, M. Ordered Mesoporous Materials in the Context of Drug Delivery Systems and Bone Tissue Engineering. *Chem. - Eur. J.* **2006**, *12*, 5934−5943.
(16) Tang, F. Q.; Li, L. L.; Chen, D. Mesoporous Silica Nanoparticles: Synthesis, Biocompatibility and Drug Delivery. *Adv. Mater.* **2012**, *24*, 1504−1534.
(17) Feng, W.; Nie, W.; He, C. L.; Zhou, X. J.; Chen, L.; Qiu, K. X.; Wang, W. Z.; Yin, Z. Q. Effect of pH-Responsive Alginate/Chitosan Multilayers Coating on Delivery Efficiency, Cellular Uptake and Biodistribution of Mesoporous Silica Nanoparticles Based Nanocarriers. *ACS Appl. Mater. Interfaces* **2014**, *6*, 8447−8460.
(18) Feng, W.; Zhou, X. J.; He, C. L.; Qiu, K. X.; Nie, W.; Chen, L.; Wang, H. S.; Mo, X. M.; Zhang, Y. Z. Polyelectrolyte Multilayer Functionalized Mesoporous Silica Nanoparticles for pH-Responsive Drug Delivery: Layer Thickness-Dependent Release Profiles and Biocompatibility. *J. Mater. Chem. B* **2013**, *1*, 5886−5898.
(19) Sun, J. D.; Liu, X. Y.; Meng, L.; Wei, W.; Zheng, Y. F. One-Step Electrodeposition of Self-Assembled Colloidal Particles: A Novel Strategy for Biomedical Coating. *Langmuir* **2014**, *30*, 11002−11010.
(20) Wu, L. Q.; Gadre, A. P.; Yi, H. M.; Kastantin, M. J.; Rubloff, G. W.; Bentley, W. E.; Payne, G. F.; Ghodssi, R. Voltage-Dependent Assembly of the Polysaccharide Chitosan onto an Electrode Surface. *Langmuir* **2002**, *18*, 8620−8625.
(21) Besra, L.; Liu, M. L. A Review on Fundamentals and Applications of Electrophoretic Deposition (EPD). *Prog. Mater. Sci.* **2007**, *52*, 1−61.
(22) Wang, Y.; Zhang, W. L.; Zhang, J. X.; Sun, W.; Zhang, R. Y.; Gu, H. C. Fabrication of a Novel Polymer-Free Nanostructured Drug-Eluting Coating for Cardiovascular Stents. *ACS Appl. Mater. Interfaces* **2013**, *5*, 10337−10345.
(23) Hu, R.; Lin, C. J.; Shi, H. Y.; Wang, H. Electrochemical Deposition Mechanism of Calcium Phosphate Coating in Dilute Ca-P Electrolyte System. *Mater. Chem. Phys.* **2009**, *115*, 718−723.
(24) Lu, X.; Leng, Y.; Zhang, Q. Y. Electrochemical Deposition of Octacalcium Phosphate Micro-Fiber/Chitosan Composite Coatings on Titanium Substrates. *Surf. Coat. Technol.* **2008**, *202*, 3142−3147.
(25) Farrokhi-Rad, M.; Shahrabi, T. Effect of Suspension Medium on the Electrophoretic Deposition of Hydroxyapatite Nanoparticles and Properties of Obtained Coatings. *Ceram. Int.* **2014**, *40*, 3031−3039.
(26) He, C. L.; Xiao, G. Y.; Jin, X. B.; Sun, C. H.; Ma, P. X. Electrodeposition on Nanofibrous Polymer Scaffolds: Rapid Mineralization, Tunable Calcium Phosphate Composition and Topography. *Adv. Funct. Mater.* **2010**, *20*, 3568−3576.
(27) He, C. L.; Jin, X. B.; Ma, P. X. Calcium Phosphate Deposition Rate, Structure and Osteoconductivity on Electrospun Poly(L-Lactic Acid) Matrix Using Electrodeposition or Simulated Body Fluid Incubation. *Acta Biomater.* **2014**, *10*, 419−427.
(28) He, C. L.; Zhang, F.; Cao, L. J.; Feng, W.; Qiu, K. X.; Zhang, Y. Z.; Wang, H. S.; Mo, X. M.; Wang, J. W. Rapid Mineralization of Porous Gelatin Scaffolds by Electrodeposition for Bone Tissue Engineering. *J. Mater. Chem.* **2012**, *22*, 2111−2119.
(29) Chen, T. L. Inhibition of Growth and Differentiation of Osteoprogenitors in Mouse Bone Marrow Stromal Cell Cultures by Increased Donor Age and Glucocorticoid Treatment. *Bone* **2004**, *35*, 83−95.
(30) Ma, X. L.; Zhang, X. P.; Jia, Y. F.; Zu, S. S.; Han, S. Y.; Xiao, D. J.; Sun, H. J.; Wang, Y. S. Dexamethasone Induces Osteogenesis Via Regulation of Hedgehog Signalling Molecules in Rat Mesenchymal Stem Cells. *Int. Orthop.* **2013**, *37*, 1399−1404.
(31) de Matos, M. B. C.; Piedade, A. P.; Alvarez-Lorenzo, C.; Concheiro, A.; Braga, M. E. M.; de Sousa, H. C. Dexamethasone-Loaded Poly(ε-Caprolactone)/Silica Nanoparticles Composites Prepared by Supercritical CO_2 Foaming/Mixing and Deposition. *Int. J. Pharm.* **2013**, *456*, 269−281.
(32) Yang, Y. J.; Tao, X.; Hou, Q.; Chen, J. F. Fluorescent Mesoporous Silica Nanotubes Incorporating CdS Quantum Dots for Controlled Release of Ibuprofen. *Acta Biomater.* **2009**, *5*, 3488−3496.
(33) Kim, K.; Dean, D.; Mikos, A. G.; Fisher, J. P. Effect of Initial Cell Seeding Density on Early Osteogenic Signal Expression of Rat Bone Marrow Stromal Cells Cultured on Cross-Linked Poly(propylene fumarate) Disks. *Biomacromolecules* **2009**, *10*, 1810−1817.
(34) Zhang, J. H.; Zhao, S. C.; Zhu, Y. F.; Huang, Y. J.; Zhu, M.; Tao, C. L.; Zhang, C. Q. Three-Dimensional Printing of Strontium-containing Mesoporous Bioactive Glass Scaffolds for Bone Regeneration. *Acta Biomater.* **2014**, *10*, 2269−2281.
(35) Peng, H. J.; Yin, Z.; Liu, H. H.; Chen, X.; Feng, B.; Yuan, H. H.; Su, B.; Ouyang, H. W.; Zhang, Y. Z. Electrospun Biomimetic Scaffold of Hydroxyapatite/Chitosan Supports Enhanced Osteogenic Differentiation of mMSCs. *Nanotechnology* **2012**, *23*, 485102.
(36) Thormann, U.; Ray, S.; Sommer, U.; Elkhassawna, T.; Rehling, T.; Hundgeburth, M.; Henss, A.; Rohnke, M.; Janek, J.; Lips, K. S.; Heiss, C.; Schlewitz, G.; Szalay, G.; Schumacher, M.; Gelinsky, M.; Schnettler, R.; Alt, V. Bone Formation Induced by Strontium Modified Calcium Phosphate Cement in Critical-Size Metaphyseal Fracture Defects in Ovariectomized Rats. *Biomaterials* **2013**, *34*, 8589−8598.
(37) Wei, G. B.; Ma, P. X. Partially Nanofibrous Architecture of 3D Tissue Engineering Scaffolds. *Biomaterials* **2009**, *30*, 6426−6434.
(38) Qiu, K. X.; He, C. L.; Feng, W.; Wang, W. Z.; Zhou, X. J.; Yin, Z. Q.; Chen, L.; Wang, H. S.; Mo, X. M. Doxorubicin-loaded Electrospun Poly(L-Lactic Acid)/Mesoporous Silica Nanoparticles Composite Nanofibers for Potential Postsurgical Cancer Treatment. *J. Mater. Chem. B* **2013**, *1*, 4601−4611.
(39) Yuan, L.; Tang, Q. Q.; Yang, D.; Zhang, J. Z.; Zhang, F. Y.; Hu, J. H. Preparation of pH-Responsive Mesoporous Silica Nanoparticles and Their Application in Controlled Drug Delivery. *J. Phys. Chem. C* **2011**, *115*, 9926−9932.
(40) Nguyen, L. T. H.; Liao, S. S.; Chan, C. K.; Ramakrishna, S. Electrospun Poly(L-Lactic Acid) Nanofibres Loaded with Dexamethasone to Induce Osteogenic Differentiation of Human Mesenchymal Stem Cells. *J. Biomater. Sci. Polym. Ed.* **2012**, *23*, 1771−1791.
(41) Dhanyamraju, R. Impaired Calcification around Matrix Vesicles of Growth Plate and Bone in Alkaline Phosphatase-Deficient Mice (Vol 164, Pg 841, 2004). *Am. J. Pathol.* **2004**, *164*, 1873.
(42) Liu, Y.; Porta, A.; Peng, X. R.; Gengaro, K.; Cunningham, E. B.; Li, H.; Dominguez, L. A.; Bellido, T.; Christakos, S. Prevention of Glucocorticoid-Induced Apoptosis in Osteocytes and Osteoblasts by Calbindin-D_{28k}. *J. Bone Miner. Res.* **2004**, *19*, 479−490.
(43) Hong, D.; Chen, H. X.; Xue, Y.; Li, D. M.; Wan, X. C.; Ge, R. S.; Li, J. C. Osteoblastogenic Effects of Dexamethasone through Upregulation of TAZ Expression in Rat Mesenchymal Stem Cells. *J. Steroid Biochem. Mol. Biol.* **2009**, *116*, 86−92.
(44) Nguyen, L. T. H.; Liao, S.; Ramakrishna, S.; Chan, C. K. The Role of Nanofibrous Structure in Osteogenic Differentiation of Human Mesenchymal Stem Cells with Serial Passage. *Nanomedicine* **2011**, *6*, 961−974.
(45) Cao, L.; Yang, F.; Liu, G. W.; Yu, D. G.; Li, H. W.; Fan, Q. M.; Gan, Y. K.; Tang, T. T.; Dai, K. R. The Promotion of Cartilage Defect Repair Using Adenovirus Mediated Sox9 Gene Transfer of Rabbit Bone Marrow Mesenchymal Stem Cells. *Biomaterials* **2011**, *32*, 3910−3920.
(46) Xue, J. X.; Gong, Y. Y.; Zhou, G. D.; Liu, W.; Cao, Y. L.; Zhang, W. J. Chondrogenic Differentiation of Bone Marrow-Derived

DOI: 10.1021/acsami.5b11879
ACS Appl. Mater. Interfaces 2016, 8, 4137−4148

Mesenchymal Stem Cells Induced by Acellular Cartilage Sheets. *Biomaterials* **2012**, *33*, 5832−5840.

DOI: 10.1021/acsami.5b11879
ACS Appl. Mater. Interfaces 2016, 8, 4137−4148